Characterization of the lutetium-yttrium orthosilicate scintillating crystals for the CMS experiment

M. Campana(¹)(²)

(¹) *INFN, Sezione di Roma - Roma, Italy*
(²) *Dipartimento di Fisica, Sapienza Università di Roma - Roma, Italy*

Summary. — The Compact Muon Solenoid (CMS) detector is undergoing an extensive Phase II upgrade program to prepare for the challenging conditions of the High-Luminosity LHC starting in 2027. In particular, a new timing detector, the Mip Timing Detector (MTD) will measure minimum ionizing particles with a time resolution of 30–50 ps. The technology selected for the central part of the detector, the Barrel Timing Layer, consists of scintillating crystals of lutetium yttrium orthosilicate doped with cerium (LYSO:Ce) read out with Silicon Photo-Multipliers. A study of the performances of LYSO samples from different producers has been performed last year in Rome; in this report the experimental setup is described and the optical measurements are presented.

1. – Introduction

In view of the High Luminosity LHC (HL-LHC) phase, which will start operation in 2027, the Compact Muon Solenoid (CMS) experiment is foreseeing an upgrade of the detector to cope with the new challenges of HL-LHC such as an extremely high number of concurrent collisions per bunch crossing and the harsh radiation levels to which the detector will be exposed.

As part of this upgrade, CMS is planning to build the Mip Timing Detector (MTD), a novel sub-detector with the capability of tagging charged particles with a time resolution of 30–60 ps. It will be placed between the last Tracker layer and the Electromagnetic Calorimeter (ECAL).

The MTD resolution was targeted to ensure CMS operation with similar event reconstruction performance to the current one running at LHC. The MTD will be divided into two sub-detectors: the Barrel Timing Layer (BTL) and the Endcap Timing Layer (ETL). This article describes the characterization of LYSO crystal bars of the MTD BTL. The basic elements of the BTL are lutetium-yttrium orthosilicate scintillating crystals doped with cerium (LYSO:Ce), coupled with Silicon Photo-Multipliers (SiPMs) at the

two short ends. This particular kind of crystal is chosen due to LYSO high radiation hardness, that will allow to endure the radiation level of the HL-LHC phase.

2. – LYSO characteristics

LYSO is an acronym for lutetium yttrium orthosilicate ($Lu_{(2-x)}Y_xSiO_5$: Ce), with Ce standing for a crystal doped with cerium. Because of their high stopping power and fast bright scintillation, LYSO crystals have attracted a broad interest in the high energy physics community for future experiments. In addition these crystals are not very expensive and can suffer a high radiation level before their key characteristics are worsened by the damage due to radiation [1-4]. This scintillator is commonly used in medical imaging applications (*e.g.*, Positron Emission Tomography, PET), making it a well studied material.

The effective atomic number of LYSO(Ce) is 66 and its density is $7.15 \, g/cm^3$, a value greater than other crystals (table I). The LYSO characteristic high density provides high interaction rate of incoming MIP per unit of path, making it possible to minimize the thickness of the detector. Moreover the material has also a critical angle for total internal reflection of $\theta \sim 56°$. It has a fast response (100 ps rise time and 40 ns decay time), and a high light yield ($\sim$40000 photoelectrons/MeV).

The key feature of LYSO:Ce is its radiation tolerance, which is required for operation without significant loss of transparency or light output in a high radiation environment. Furthermore radiation damage in LYSO crystals recovers very slow at room temperature but can be cured by thermal annealing at $300 \, °C$ for several hours. The radiation resistance of LYSO has been studied by irradiating LYSO bars with 24 GeV protons to a fluence of $2.5 \cdot 10^{13} \, cm^{-2}$ (which is above $\sim 1 \cdot 10^{13} \, cm^{-2}$, the integrated expected level for BTL at the end of LHC for the BTL) and measuring the transparency at different wavelength before and after their exposure [5]. The result of this study is an excellent radiation tolerance of LYSO, shown in fig. 1. Indeed a negligible loss in transparency, T, is shown, corresponding to an induced absorption coefficient $\mu_{ind} = \frac{1}{L} \ln \frac{T_{before}}{T_{after}} = 0.5 \, m^{-1}$ at $\lambda = 420 \, nm$, where L is the length of the crystal.

TABLE I. – *Properties of some crystal scintillators.*

	Density [g/cm^3]	Decay time [ns]	Light yield [photons/MeV]	Energy resolution at 511 keV [%]
BGO	7.15	300	6000	10.2
LYSO(Ce)	7.1	45	40000	7.5
LaBr$_3$(Ce)	5.1	16	63000	2.9
NaI(Tl)	3.7	230	38000	6.6
BaF$_2$	4.9	0.8	12000	11.4
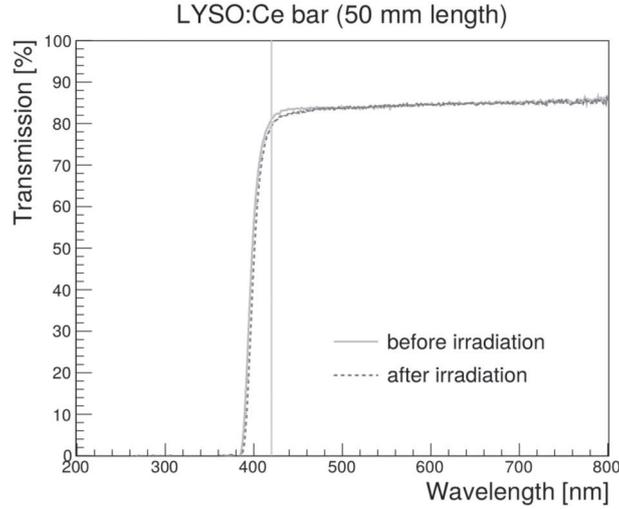
Fig. 1. – LYSO transmission as a function of wavelength before and after the irradiation; the vertical line is at 420 nm, corresponding to the peak of the SiPM spectral sensitivity.

3. – Measurements strategy

The experimental bench uses LYSO bar crystal coupled with a photo-multiplier (PMT) and the signal is acquired by a digitizer (DRS4). The single photo-electron response, calibrated using a pulsed, fast, blue LED, can be measured with the PMT and the full shape of the waveform can be accessed. Therefore, using a radioactive source with monochromatic photon emission (a ^{22}Na source), the light output at the crystal end surface can be measured. The decay time is measured by fitting the pulse shape of the crystal with a decreasing exponential. A reference crystal is used to study the stability of the measurements.

4. – Experimental setup

The light output of single crystal bars from each vendor has been measured with an experimental setup consisting of a 51 mm diameter end window photo-multiplier (ET Enterprised model 9256B) placed inside a black painted box, whose temperature has been regulated using a LAUDA RE220 chiller.

The single photo-electron response is calibrated using a pulsed, fast, blue LED. The LED pulser amplitude has been adjusted to obtain on average 1–2 photo-electrons per event (pulse length 20 ns, frequency 10 kHz). The average PDE of the PMT integrated over the LYSO spectrum, as taken from the specifications, is about 25%. Figure 2 shows a scheme of the experimental setup.

The light output has been measured by detecting one of the two 511 keV photons from a ^{22}Na source and looking at the corresponding photoelectric peak in the crystal. Single crystals are placed in a white 3D printed polylactic acid holder of 57 mm length; the holder has four holes with different transverse size and allows to support crystals vertically on the PMT entrance window. The holder also acts as an optical window.

The crystal end face on the opposite side of the PMT is not wrapped and in contact with air. The crystal is placed without any additional wrapping inside the holder in order
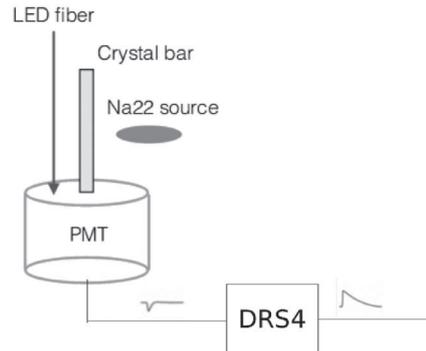
Fig. 2. – Scheme of the experimental setup: the crystal bar is placed on PMT inside a 3D printed support.

to improve the reproducibility of the light output measurement; for the same reason no optical grease is used between the crystal and the PMT glass window entrance.

The bars of the three geometries have the same length (57 mm) and width (3 mm), while the thicknesses are different (respectively 3.75 mm, 3.00 mm and 2.40 mm). The radioactive source is placed on the side of the 3D printed support.

The signal from the PMT is acquired using a DRS4 evaluation board, working at a sampling rate of 2 GS/s; this allows an integration window for the PMT signal extending up to 500 ns (each event consists of 1024 samples). A simple integration of the samples acquired by the DRS4, after subtracting the baseline value, is performed in order to obtain the integrated charge of the PMT signal. A similar procedure is followed both for the LED and SOURCE runs with different triggering conditions and integration windows: the trigger for the LED runs is obtained from the synchronisation output of the LED pulser and an integration window of 30 ns is used, while for the SOURCE runs a trigger threshold at 30 mV is set on the PMT signal and the integration window is 450 ns. The photo-electron response calibration consists in taking five LED runs, acquired with increasing LED pulse intensity; the corresponding spectra are then fitted simultaneously with the single photo-electron charge value taken as common free parameter, in order to minimise its systematic uncertainty.

5. – Experimental methods

5`1. *Single photo-electron calibration.* – The operation principle of a photo-multiplier tube is illustrated in fig. 3. Ideally a single photon absorbed in the photo-cathode liberates one photo-electron in the vacuum in the tube, and is then accelerated towards and the first dynode and focused on it. Actually not every single absorbed photon will release a photo-electron. The probability of photo-emission is quantified by the PDE, which is defined as the ratio between the number of output electrons and the number of incident photons which depends on several parameters specific to the photo-cathode material such as the reflection coefficient, full absorption coefficient of photons, the work function and also on the energy of the incident photon.

Then a number, δ_1, of secondary electrons are emitted from the first dynode that go further in the multiplication process eventually delivering a charge pulse at the anode output. When a pulse of light is incident on a PMT, the number of detected photons is determined by Poisson statistics. Being μ the average number of detected photons per
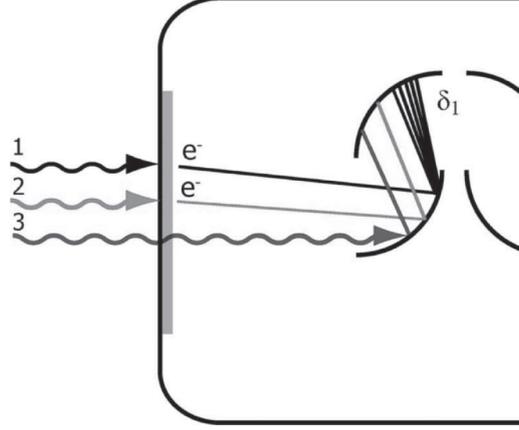
Fig. 3. – The operation principle of a photo-multiplier tube. Photon 1 creates a photo-electron at the photo-cathode that creates δ_1 secondary electrons at the first dynode. Photon 2 creates a photo-electron at the photo-cathode that is back-scattered at the first dynode to the next dynode without making secondary electrons. Photon 3 goes through the photo-cathode to create one photo-electron at the first dynode.

LED pulse, the distribution $P_\mu(n)$ in that number is given by

$$(1) \qquad P_\mu(n) = \frac{\mu^n e^{-\mu}}{n!}.$$

The response of a multiplicative dynode system to a single photo-electron follows a Poisson distribution. If the amplification of the first dynode is large (>4), the function can be approximated by a Gaussian distribution,

$$(2) \qquad G_n(x) = \frac{1}{\sigma_1\sqrt{2\pi}} \exp\left(-\frac{(x - nQ_1)^2}{2\sigma_1^2}\right),$$

where x is the charge, Q_1 is the average charge at the PMT output when one electron is collected by the first dynode, σ_1 is the corresponding standard deviation of the charge distribution and n is the number of photo-electrons collected by the first dynode. The response of the PMT is the convolution of eq. (1) and eq. (2):

$$(3) \qquad S(x) = P(n, \mu) \otimes G_n(x) = N \sum_{n=0}^{\infty} \frac{\mu^n e^{-\mu}}{n!} \frac{1}{\sigma_n \sqrt{2n\pi}} \exp\left(-\frac{(x - Q_n)^2}{2\sigma_n^2}\right),$$

where N is a normalization factor, $Q_n = Q_0 + nQ_1$, $\sigma_n = \sqrt{\sigma_0^2 + n\sigma_1^2}$, while Q_0 and σ_0 are respectively the mean and the RMS of the pedestal distribution. In fig. 4, a typical LED spectrum is shown. The fitting function used to parameterize the spectrum is given by eq. (3).

5˙2. *Light output*. – The strategy to measure the light output is related to the measurement of the energy deposited in the crystal by monochromatic photons, coming from a radioactive source and interacting via photoelectric effect in the crystal. By reconstructing the crystal energy spectrum irradiated by a radioactive source, the value of the
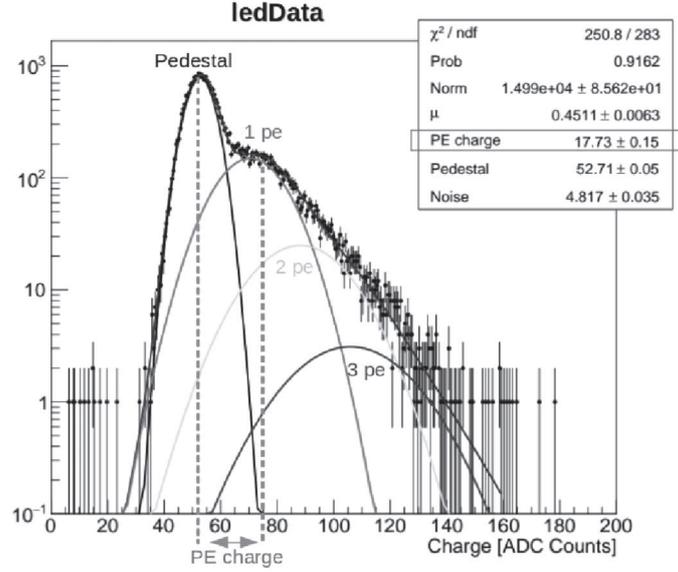
Fig. 4. – Typical LED spectrum; the black line is the pedestal contribution to the fitting function, while the single–photo-electron, two– and three–photo-electron contributions are shown in different gray scales.

photoelectric peak, in ADC counts, can be measured for a photon of known energy (E). In fact, given an incident photon with energy E absorbed in the bar,

$$(4) \qquad E\,[\text{ADC}] \propto PE \cdot PDE \cdot LO,$$

where PE is the single photo-electron value, LO is the light output.

The analysis of the relative light output is based on the measurement of a crystal and the measurement of the reference crystal. The reference crystal is measured every day, in order to monitor the stability of the electronic and of the PMT. Then, given the ratio between the photoelectric peak value of the crystal and the photoelectric peak value of the reference crystal, the measurement is reported as $\frac{E_{\text{bar}}}{E_{\text{ref}}}$. Since the factors PE and PDE are equal in both cases because the electronic system and the geometry are the same, the ratio

$$(5) \qquad \frac{E_{\text{bar}}}{E_{\text{ref}}} = \frac{LO_{\text{bar}}}{LO_{\text{ref}}},$$

which represents the relative LO measurement.

The light output measurement consists of calibration of the PE value and measurement of a test crystal. Then, given the PE value (E_{pe}) and the photoelectric peak value in the crystal (E_{bar}), the measurement is reported as:

$$(6) \qquad LO = \frac{E_{\text{bar}}}{E_{\text{pe}}} \frac{1}{E \cdot PDE}$$

The radioactive source used for these measurements is the ^{22}Na and fig. 5 shows an example of the typical ^{22}Na spectrum.

χ^2 / ndf	190.8 / 181
Prob	0.295
p0	19.5 ± 3.5
p1	0.002944 ± 0.000886
p2	1.613e+04 ± 1.421e+02
p3	1.343 ± 0.224
p4	1.885e+04 ± 5.232e+01
p5	834.9 ± 70.5
p6	11.03 ± 3.47
p7	0.0003424 ± 0.0000261
p8	6057 ± 967.9
p9	20.78 ± 3.76
p10	7516 ± 14.1
p11	576.9 ± 15.6
p12	2598 ± 65.9
p13	12.74 ± 1.24
p14	2.041 ± 0.691
p15	4384 ± 102.8
p16	697.8 ± 146.6
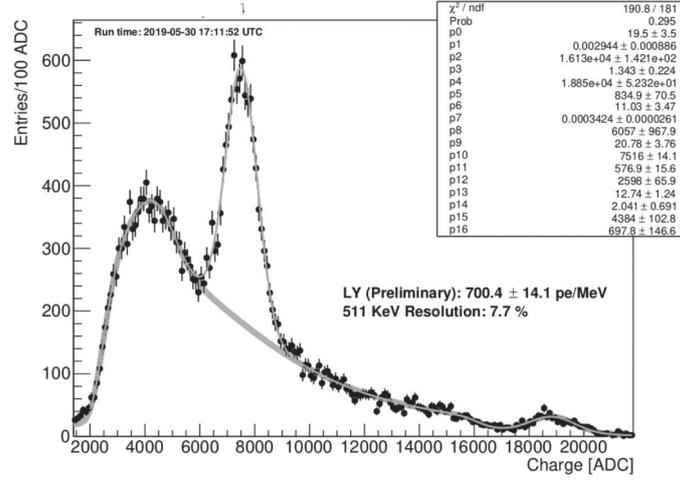
Fig. 5. – Example of ^{22}Na spectrum, the charge in the x-axis is in Analogue to Digital Converter (ADC) counts. The spectrum fitting function and a fitting function without the 511 keV peak are shown.

5˙3. *Decay time*. – The acquisition with a fast sampling digitizer allows the extraction of the scintillation decay time directly from the acquired waveform of the PMT signal; an average over all PMT signals with an associated total charge above roughly 100 keV in the ^{22}Na runs is performed. The average waveform is passed through a Butterworth filter with a cut-off frequency of 20 MHz to reduce oscillations due the imperfect impedance matching between the PMT anode output and the DRS4 buffer input. The decay time is extracted from a fit which includes a single exponential decay function and a Gaussian turn-on. In fig. 6, the pulse shape of a LYSO crystal is shown. The rise time of the signal is not fitted since it is dominated by the PMT rise time (few ns), while the LYSO one is
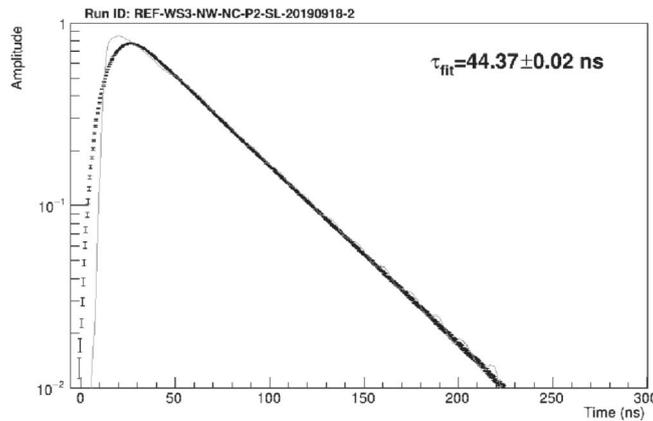
Fig. 6. – Waveform of LYSO bar. The black dots are the filtered data, while the line is the waveform before the Butterworth filter is applied to the data. The black line is the fit performed on the filtered data.

TABLE II. – *Crystal producers in alphabetic order.*

Producer name	Number of crystals
Crystal Photonics	15
Hypercrystal	15
JT Crystal Technology	15
Shanghai Institute of Ceramics	15
Simcrystals Technology	15
SIPAT	15
Tianle Photonics	15
Zecotek	10

$\sim$100 ps. Data have been fitted with the following function:

$$(7) \qquad f(x) = p_0 \left(\exp\left(\frac{-2p_1 \cdot (x - p_3) + p_2^2}{2p_1^2} \right) \cdot \left(1 - \mathrm{Erf}\left(\frac{p_1 \cdot (x - p_3) + p_2^2}{\sqrt{2}p_1 \cdot p_2} \right) \right) \right),$$

where the exponential part of the fitting function describes the peak and the decay of the signal, while the error function parametrizes the rise and the peak of the signal. In particular, the parameter p_1 corresponds to the decay time of the LYSO bars.

6. – Results

In Rome, samples from 8 different worldwide producers, reported in table II, have been provided to characterize different crystals. The crystals of these producers have 3 different geometries, corresponding to the BTL ones.

The light output mean has a total spread of about 15% from the smallest to the highest producer yield. The spread of the light output from different samples of the same producer is, for most of the producers, around 4%, thus compatible with the reproducibility of the measurement itself, as can be seen in fig. 7. All the crystals from the several producers satisfy the light output CMS requirements for the BTL.

Figure 8 shows the decay time of crystals from the different producers as a function of the light output normalised to the reference crystal. Most crystals have a decay time of 43–45 ns, however crystals from two producers have a decay time slightly smaller ($\sim$40 ns) than the others, while crystals from one producer have a decay time higher than the others ($\sim$47 ns).
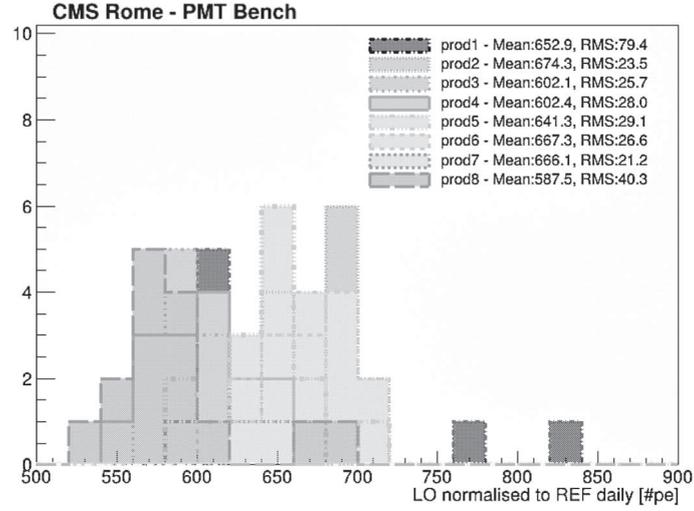
Fig. 7. – Light output from different producers normalised to the daily light output measurement of the reference crystal. Each vendor is represented with a different scale of grey. The numbering of the producers of table II is assigned randomly.

7. – Conclusion

To face all the challenges of High Luminosity LHC, CMS will build a new detector (MIP Timing Detector) with the purpose of obtaining a time resolution of 30 ps for charged particles. The Barrel Timing Layer (BTL) will be made by LYSO:Ce crystal bars readout by SiPMs.

This article describes the measurement campaign, performed in 2019 in Rome, aimed at characterizing LYSO crystal bars for the BTL detectors. Eight different producers
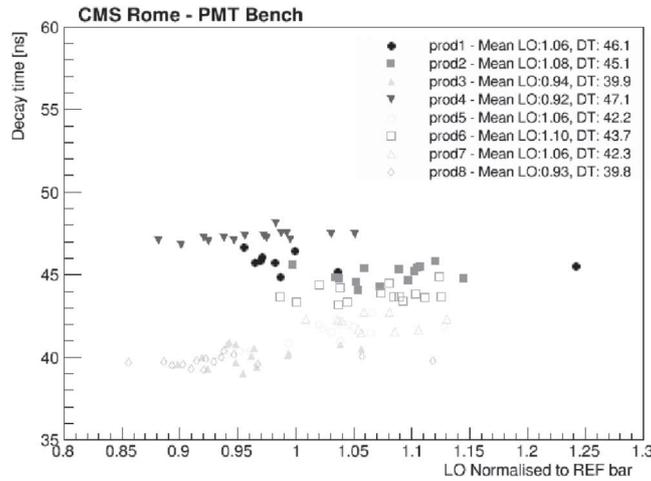
Fig. 8. – Decay time as a function of light output for different producers. The light output measurements are normalised to the daily light output measurement of the reference crystal. Each vendor is represented with a different marker.

have been involved in this campaign; each of them provided 15 bars (five bars for each BTL geometry).

On the basis of these measurements, the following conclusions on the crystal properties have been reached:

- The decay time of a crystal bar is similar among different producers going from 40 to 47 ns.

- The light output mean has a total spread of about 15% from the smallest to the highest producer yield.

To complete the measurement campaign few bars for each producer will be irradiated with ^{60}Co, at the ENEA-Casaccia Calliope facility, to test the resistance to the radiation corresponding to the full HL-LHC integrated dose.

* * *

REFERENCES

[1] CHEN J., MAO R., ZHANG L. and ZHU R., *IEEE Trans. Nucl. Sci.*, **54** (2007) 1319.
[2] ZHANG LIYUAN, MAO RIHUA, YANG FANG and ZHU REN-YUAN, *IEEE Trans. Nucl. Sci.*, **61** (2014) 483.
[3] YANG FAN, ZHANG LIYUAN, ZHU REN-YUAN, KAPUSTINSKY JON, NELSON RON, and WANG ZHEHUI, *Nucl. Instrum. Methods Phys. Res. Sect. A*, **824** (2016) 726.
[4] AUFFRAY ETIENNETTE, BARYSEVICH A., FEDOROV A., KORZHIK MIKHAIL, KOSCHAN MERRY, LUCCHINI MARCO, MECHINSKY VITALY, MELCHER CHUCK and VOITOVICH A., *Nucl. Instrum. Methods Phys. Res. Sect. A*, **721** (2013) 76.
[5] CMS COLLABORATION, *A MIP Timing Detector for the CMS Phase-2 Upgrade*, https://cds.cern.ch/record/2296612/files/LHCC-P-009.pdf.